photonics

MDPI

Article

Exceptional Points in Hermitian Media, and Density of States Singularities in Anisotropic, Tellegen, Chiral, Moving-Medium, Omega and Other Isotropy-Broken Materials

Maxim Durach

Center for Advanced Materials Science, Department of Biochemistry, Chemistry and Physics, Georgia Southern University, Statesboro, GA 30460, USA; mdurach@georgiasouthern.edu

Abstract

Anisotropic, Tellegen, chiral, moving-medium-type, omega, gyrotropic, hyperbolic, and multi-hyperbolic materials form an important class of isotropy-broken photonic media in which wave propagation can no longer be characterized by the Fresnel wave surface alone. Here we show that Fresnel wave surfaces can be converted into propagation maps that organize positive- and negative-phase-velocity propagation together with attenuation and amplification. In Hermitian media, the boundary between forward and backward propagation forms the orthogonal-phase-velocity separatrix. This separatrix is also a continuous locus of orthogonal-phase-velocity exceptional points, where the index-of-refraction operator becomes defective even though the material medium remains Hermitian. In non-Hermitian media, the attenuation–amplification boundary forms the loss–gain separatrix. The associated loss–gain singularities occur where the handedness remains continuous while the gain–loss character changes sign. Their physical importance is revealed by the momentum-resolved density of states: at these points, the Lorentzian linewidth of the non-Hermitian momentum-resolved density of states (DOS) collapses, producing sharp DOS peaks whose sign reverses across the separatrix. Thus, loss–gain singularities are threshold-like singularities of the Fresnel wave-surface propagation map, generated by non-Hermitian linewidth collapse. The result is a compact geometric language for describing how handedness, degeneracy, loss, gain, and momentum-resolved DOS are organized in isotropy-broken electromagnetic materials.

Keywords: exceptional points; density of states; negative refraction; metamaterials; non-Hermitian materials; anisotropic materials; bianisotropic materials; Tellegen coupling; Artificial Moving Materials; diabolic singularities

Check for updates

Received: 11 May 2026
Revised: 3 June 2026
Accepted: 10 June 2026
Published: 14 June 2026

Copyright: © 2026 by the author. Licensee MDPI, Basel, Switzerland. This article is an open access article distributed under the terms and conditions of the Creative Commons Attribution (CC BY) license.

1. Introduction

Modern photonics now encompasses a remarkably broad class of electromagnetic media, including isotropic and anisotropic dielectric, plasmonic, magnetic, gyroelectric and gyromagnetic systems, hyperbolic and multi-hyperbolic materials, and a wide range of bianisotropic responses such as chiral, Tellegen, omega, moving-medium, and axion-type couplings [1–14]. In parallel, contemporary research increasingly extends into non-Hermitian platforms, where loss and gain fundamentally reshape wave propagation [15–18]. In all these cases, the allowed plane-wave states are organized by the Fresnel wave surface, whose geometry encodes the directional structure of propagation in momentum space [18–20]. Over the past decade, Fresnel surfaces have emerged as a central organizing object in

photonics, supporting classifications based on topology, asymptotic high-k structure, and singular degeneracies. In particular, the high-k taxonomy introduced by Durach organizes materials into non-, mono-, bi-, tri-, and tetra-hyperbolic phases according to the number of asymptotic double-cone branches [9], while the framework of Favaro and Hehl emphasizes diabolical points at which polarization sheets intersect [21]. At the level of singularities, the standard distinction is between Hermitian diabolical points, where eigenvalues coincide but eigenvectors remain independent, and non-Hermitian exceptional points, where both eigenvalues and eigenvectors coalesce into a defective Jordan structure [22–25].

Despite the power of these classifications, they do not incorporate two physical attributes that are fundamental to electromagnetic wave propagation in complex media. The first is the handedness of the waves and the phase flow relative to energy transport, quantified by the sign of $\boldsymbol{k} \cdot \boldsymbol{S}$, where $\boldsymbol{k}$ is the wavevector and $\boldsymbol{S}$ is the time-averaged Poynting vector. This criterion distinguishes positive-phase-velocity (PPV), negative-phase-velocity (NPV), and orthogonal-phase-velocity (OPV) propagation and becomes especially important in isotropy-broken, bianisotropic, gyrotropic, and multi-hyperbolic systems [26]. The second is the gain–loss character of the waves in non-Hermitian media, encoded in the imaginary part of the refractive index, or equivalently in the sign of $\mathrm{Im}(\boldsymbol{k}) \cdot \boldsymbol{S}$, which distinguishes attenuation from amplification [18,27]. Existing isofrequency wave-surface classifications consider topology, sheet connectivity, asymptotic cones, and degeneracies, but the organization of the Fresnel wave surface into propagation domains of handedness and gain–loss has not been previously studied.

In this work, we show that Fresnel wave surfaces in Hermitian and non-Hermitian media can be naturally converted into propagation maps. Two scalar functions, $\mathrm{Re}(\boldsymbol{k}) \cdot \boldsymbol{S}$ and $\mathrm{Im}(\boldsymbol{k}) \cdot \boldsymbol{S}$, divide the surface into four distinct sectors corresponding to PPV with loss, PPV with gain, NPV with loss, and NPV with gain. Using the spherical coordinates in momentum space the real part of the refractive index n is positive, and the component of the Poynting vector along the propagation direction, s, is positive for PPV $(s > 0)$ and negative for NPV $(s < 0)$. Writing the complex refractive index as $n \to n + i\kappa$, where $\kappa = \mathrm{Im}(n)$, the sign of κ determines attenuation or amplification through its relation to s: $\kappa s > 0$ corresponds to loss, while $\kappa s < 0$ corresponds to gain. The four sectors therefore correspond to PPV with loss $(s > 0, \kappa s > 0)$, PPV with gain $(s > 0, \kappa s < 0)$, NPV with loss $(s < 0, \kappa s > 0)$, and NPV with gain $(s < 0, \kappa s < 0)$. This can be seen in Figure 1a, where a Fresnel wave surface is depicted with these sectors identified. In this sense, the Fresnel surface acquires a map-like structure: it is partitioned into four neighboring domains of distinct physical behavior, reminiscent of the four-color theorem in planar map coloring, where four colors suffice to distinguish adjacent regions of a map [28]. In this way, the Fresnel wave surface is no longer viewed merely as an isofrequency surface but as a directional atlas of wave behavior, which is especially important in isotropy-broken media.

The boundaries between these domains are separatrix curves of two different kinds. In Hermitian media, the OPV condition $\boldsymbol{k} \cdot \boldsymbol{S} = 0$ separates forward and backward propagation and defines what we term orthogonal-phase-velocity separatrices. The purple curves in Figure 1a corresponds to this separatrix. These curves are geometrically natural because, as we demonstrate, they correspond to the silhouette of the Fresnel surface when viewed along $\boldsymbol{k}$, that is, to points where the Fresnel wave-surface normal is orthogonal to the viewing direction from the origin in momentum space. At the same time, they represent the locus where right-handed and left-handed propagation domains meet and touch without crossing. Because every point on this separatrix marks a touching between the conventional right-handed propagation regime and the left-handed regime, the OPV separatrix is also a continuous locus of OPV exceptional points, where the index-of-refraction operator becomes defective even though the material medium remains Hermitian.

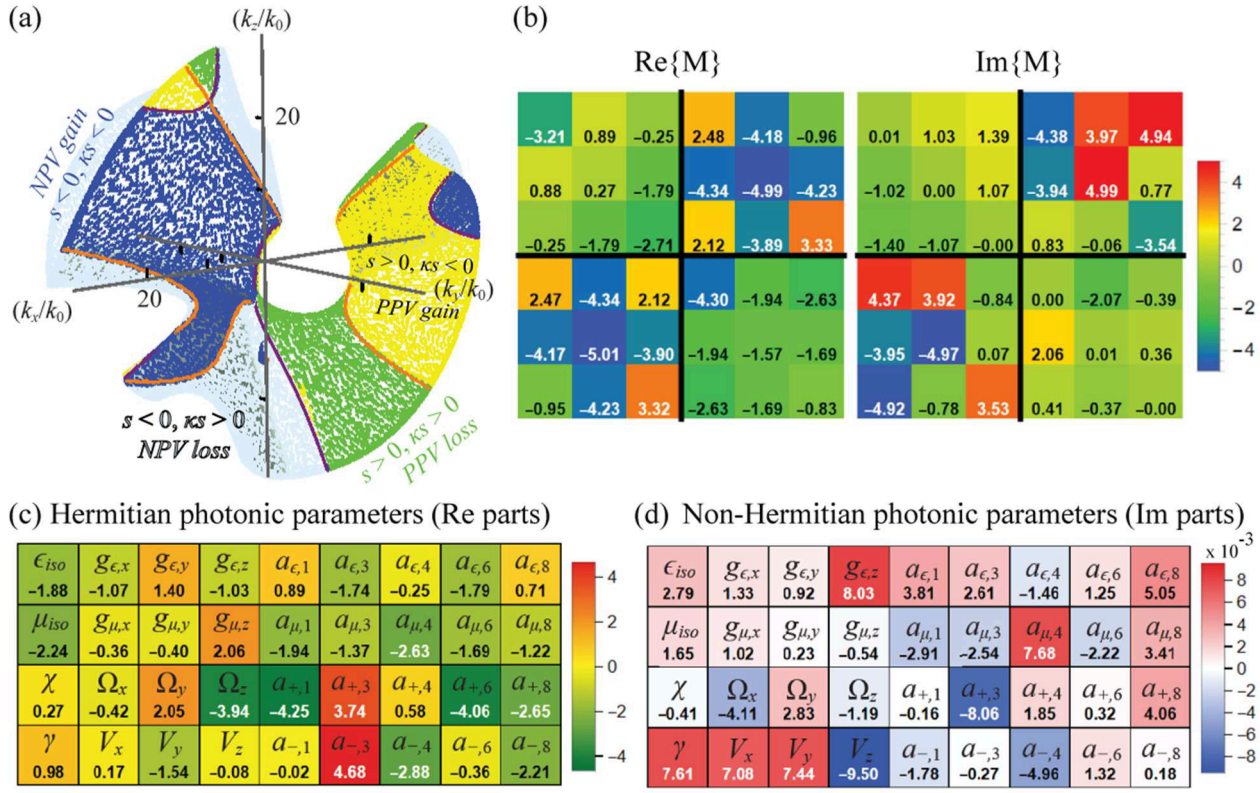


Figure 1. Fresnel wave-surface propagation map and constitutive-parameter decomposition. (**a**) A Fresnel wave surface divided into four propagation sectors according to the signs of s and κs, distinguishing PPV/NPV propagation and loss/gain behavior. The purple curve shows the OPV condition $\boldsymbol{k} \cdot \boldsymbol{S} = 0$, forming the OPV separatrix between PPV and NPV domains as a continuous locus of OPV exceptional points. (**b**) Real and imaginary parts of the constitutive matrix $\hat{M}$ generating the surface in panel (**a**). (**c**,**d**) Decomposition of $\hat{M}$ into photonic material parameters: isotropic electric and magnetic response, gyrotropy, anisotropy, Tellegen and chiral response, moving-medium and omega-type magnetoelectric coupling, and symmetric traceless magnetoelectric anisotropy.

In non-Hermitian media, the condition $\mathrm{Im}(\boldsymbol{k}) \cdot \boldsymbol{S} = 0$ separates attenuation from amplification and gives rise to what we term gain–loss separatrices. The entire gain–loss separatrix is likewise a continuous locus of gain–loss singularities, where the phase propagation remains continuous while the field passes from the dark side of the separatrix to the bright side, or vice versa. Together, these structures provide a unified framework that incorporates both wave handedness and non-Hermitian gain–loss behavior into the geometry of Fresnel wave surfaces.

To connect these geometric propagation maps to actual material design, we next express the underlying electromagnetic medium through a constitutive matrix and a photonic-parameter decomposition. Within the linear regime, diverse classes of materials are described holistically by a constitutive matrix $\hat{M}$, whose structure encodes the electromagnetic response by relating the fields in electromagnetic waves, $(\boldsymbol{D}, \boldsymbol{B})^T = \hat{M}\,(\boldsymbol{E}, \boldsymbol{H})^T$. Specifically, it is a block matrix

$$\hat{M} = \begin{pmatrix} \hat{\epsilon} & \hat{X} \\ \hat{Y} & \hat{\mu} \end{pmatrix}, \tag{1}$$

where $\hat{\epsilon}$, $\hat{\mu}$ are the permittivity and permeability and $\hat{X}$, $\hat{Y}$ are magnetoelectric couplings [6]. In Figure 1b we show the matrix $\hat{M}$ corresponding to the Fresnel wave surface from Figure 1a. Several parametrizations of $\hat{M}$ have been developed to connect its elements to underlying physical mechanisms. Notable examples include the decomposition of Hehl and Obukhov into principal, skewon, and axion parts [2] and the bianisotropy

parametrization by Michael Berry [22]. Another important line of work, by Mackay and Lakhtakia, classified constitutive dyadics according to space-time symmetry and magnetic-point-group constraints [6].

In this work, we adopt a novel photonic parametrization, which provides a systematic and physically transparent mapping between the matrix elements of the constitutive tensors and distinct coupling mechanisms. We represent the material tensors $\hat{\epsilon}$, $\hat{\mu}$, $\hat{X}$, and $\hat{Y}$ as

$$\hat{\epsilon} = \epsilon_{iso}\hat{I}_3 + i(\boldsymbol{g}_\epsilon \cdot \hat{\mathbf{S}}) + \boldsymbol{a}_\epsilon \cdot \hat{\boldsymbol{A}}, \tag{2}$$

$$\hat{\mu} = \mu_{iso}\hat{I}_3 + i\left(\boldsymbol{g}_\mu \cdot \hat{\mathbf{S}}\right) + \boldsymbol{a}_\mu \cdot \hat{\boldsymbol{A}} \tag{3}$$

$$\hat{X} = (\chi - i\gamma)\hat{I}_3 + (\boldsymbol{V} + i\boldsymbol{\Omega}) \cdot \hat{\mathbf{S}} + (\boldsymbol{a}_+ - i\boldsymbol{a}_-) \cdot \hat{\boldsymbol{A}} \tag{4}$$

$$\hat{Y} = (\chi + i\gamma)\hat{I}_3 + (-\boldsymbol{V} + i\boldsymbol{\Omega}) \cdot \hat{\mathbf{S}} + (\boldsymbol{a}_+ + i\boldsymbol{a}_-) \cdot \hat{\boldsymbol{A}} \tag{5}$$

Here, $\hat{\mathbf{S}} = i(-\lambda_7, \lambda_5, -\lambda_2)$, $\hat{\boldsymbol{A}} = (\lambda_1, \lambda_3, \lambda_4, \lambda_6, \lambda_8)$, and λ_i are Gell-Mann matrices, so that $\hat{\mathbf{S}}$ spans the antisymmetric spin-1 subspace, while $\hat{\boldsymbol{A}}$ spans the symmetric traceless subspace. The coefficients in this decomposition are obtained by direct projection onto λ_i basis matrices and therefore have a clear physical meaning.

The scalars ϵ_{iso} and μ_{iso} describe the isotropic electric and magnetic response. The vectors $\boldsymbol{g}_\epsilon$ and $\boldsymbol{g}_\mu$ describe the gyroelectric and gyromagnetic response, respectively. In the magnetoelectric part, χ is the isotropic Tellegen coupling, γ is the isotropic chiral coupling, $\boldsymbol{V}$ is the antisymmetric moving-medium-type nonreciprocal coupling, and $\boldsymbol{\Omega}$ is the antisymmetric omega-type reciprocal magnetoelectric coupling. Finally, $\boldsymbol{a}_\epsilon$ and $\boldsymbol{a}_\mu$ describe the symmetric traceless anisotropic electric and magnetic response, while $\boldsymbol{a}_+$ and $\boldsymbol{a}_-$ describe the symmetric traceless anisotropic Tellegen-type and chiral-type magnetoelectric response, respectively. In Figure 1c,d, we show the photonic parameters corresponding to the Fresnel wave surface and extracted from matrix $\hat{M}$ in Figure 1b extracted according to formulas presented in Appendix A.

One advantage of this parametrization is that it is organized by rotational symmetry. The isotropic terms are SO(3) scalars ($l = 0$), the antisymmetric terms transform as vectors ($l = 1$), and the symmetric traceless terms transform as quadrupolar tensors ($l = 2$). Consequently, the five anisotropy parameters form a real $l = 2$ tensor basis, and their behavior under rotations is governed by the corresponding Wigner rotation matrices. This parametrization allows the propagation-map sectors, OPV exceptional points, and gain–loss singularities introduced in this paper to be traced back to specific material mechanisms: isotropic response, gyrotropy, anisotropy, Tellegen/chiral response, moving-medium coupling, and omega coupling.

The propagation-map features discussed here can be approached experimentally in several existing classes of photonic media. Hyperbolic and anisotropic metamaterials provide natural platforms for observing OPV separatrices, because they support directions in momentum space where the phase velocity and energy flow become orthogonal. Chiral, omega-type, Tellegen, and more general bianisotropic metamaterials or metasurfaces provide additional control over the magnetoelectric coupling terms that enter the decomposition above. Non-Hermitian extensions can be realized by adding controlled loss, optical gain, or balanced loss–gain modulation. In such systems, the relevant measurable observables are the angular dependence of the refractive-index branches, the direction of the time-averaged Poynting vector, the sign of $\boldsymbol{k} \cdot \boldsymbol{S}$, polarization coalescence near OPV exceptional points, and the linewidth narrowing or enhancement of the momentum-resolved spectral response near gain–loss separatrices. Experimentally, these quantities may be accessed through angle-resolved transmission/reflection measurements, prism or grating coupling to high-k modes, near-field mapping of energy flow, polarization-resolved mea-

surements, and momentum-resolved spectroscopy. Thus, the present formalism provides not only a classification of Fresnel-surface geometry but also a route for identifying experimentally testable signatures in anisotropic, hyperbolic, bianisotropic, and non-Hermitian photonic platforms.

2. Index-of-Refraction Operator and Directional Photonics Parameters

To demonstrate the properties of OPV exceptional points and gain–loss singularities, we begin with Maxwell's equations in a linear medium,

$$\nabla \times \boldsymbol{H} - \frac{1}{c}\frac{\partial \boldsymbol{D}}{\partial t} = \frac{4\pi}{c}\boldsymbol{j}_e, -\nabla \times \boldsymbol{E} - \frac{1}{c}\frac{\partial \boldsymbol{B}}{\partial t} = \frac{4\pi}{c}\boldsymbol{j}_m.$$

These equations can be written in operator form as

$$\left(\hat{Q} - \frac{1}{c}\frac{\partial}{\partial t}\hat{M}\right)\begin{pmatrix}\boldsymbol{E}\\ \boldsymbol{H}\end{pmatrix} = -\frac{4\pi}{c}\begin{pmatrix}\boldsymbol{j}_e\\ \boldsymbol{j}_m\end{pmatrix},$$

with $\hat{Q} = \begin{pmatrix}\hat{0} & \nabla \times \hat{I}\\ -\nabla \times \hat{I} & \hat{0}\end{pmatrix}$. Utilizing the decomposition in Equations (2)–(5), Maxwell's equations for a plane wave with wave vector $\boldsymbol{k}$ and frequency $\omega = k_0 c$ can be written as

$$\hat{\mathcal{L}}(\boldsymbol{k})\begin{pmatrix}\boldsymbol{E}\\ \boldsymbol{H}\end{pmatrix} = \left[\hat{M}_{iso} \otimes \hat{I}_3 + \sum_{j=1}^{3}\left(\hat{M}_j^{(S)} + i\frac{k_j}{k_0}\hat{\sigma}_y\right) \otimes \hat{S}_j + \sum_{n=1}^{5}\hat{M}_n^{(A)} \otimes \hat{A}_n\right]\begin{pmatrix}\boldsymbol{E}\\ \boldsymbol{H}\end{pmatrix} = -\frac{4\pi}{ik_0 c}\begin{pmatrix}\boldsymbol{j}_e\\ \boldsymbol{j}_m\end{pmatrix}.$$

where $\hat{\sigma}_y$ is a Pauli matrix and the nine matrices $\hat{M}_i$ are

$$\hat{M}_{iso} = \begin{pmatrix}\epsilon_{iso} & \chi - i\gamma\\ \chi + i\gamma & \mu_{\text{iso}}\end{pmatrix},\ M_j^{(S)} = \begin{pmatrix}i\,g_{\epsilon j} & V_j + i\Omega_j\\ -V_j + i\Omega_j & i\,g_{\mu j}\end{pmatrix}, j = 1,2,3,$$

$$M_n^{(A)} = \begin{pmatrix}a_{\epsilon n} & a_{+n} - ia_{-n}\\ a_{+n} + ia_{-n} & a_{\mu n}\end{pmatrix}, n = 1,\ldots,5.$$

To express the field solutions in terms of the sources we use the dyadic Green's function $\hat{G}$:

$$\begin{pmatrix}\boldsymbol{E}\\ \boldsymbol{H}\end{pmatrix} = 4\pi i k_0\,\hat{G}\begin{pmatrix}\boldsymbol{j}_e\\ \boldsymbol{j}_m\end{pmatrix},\ \hat{G} = i\omega\hat{\mathcal{L}}^{-1} \tag{6}$$

In momentum space, the Green's function is

$$\hat{G}(i\boldsymbol{k}, -ik_0) = i\omega\frac{\text{adj}\ \hat{\mathcal{L}}(i\boldsymbol{k}, -ik_0)}{\det\ \hat{\mathcal{L}}(i\boldsymbol{k}, -ik_0)} \tag{7}$$

Once the material response is specified by $\hat{M}$, the Maxwell operator $\hat{\mathcal{L}}$ determines the dispersion equation for plane waves in the medium. The on-shell wavevectors are those for which the Green's function has poles, or equivalently for which the determinant of the Maxwell operator vanishes [18]. In Hermitian media, these modes are not broadened by loss or gain, so their allowed wavevectors form a sharply defined, or bare, Fresnel wave surface given by

$$F(\boldsymbol{k}) = \det\hat{\mathcal{L}}(i\boldsymbol{k}, -ik_0) = 0. \tag{8}$$

This surface is a two-dimensional manifold in momentum space with zero thickness, corresponding to the delta-functional momentum-resolved 3D density of states $\rho \propto \delta(F(\boldsymbol{k}))$. We refer to it as a bare Fresnel wave surface to emphasize the absence of non-Hermitian broadening.

To analyze the topology and polarization structure of Fresnel wave surfaces, we employ the index-of-refraction-operator method. Consider a plane wave with fields $\boldsymbol{E}, \boldsymbol{H}, \boldsymbol{D}, \boldsymbol{B} \propto e^{i(\boldsymbol{k}\cdot\boldsymbol{r}-k_0ct)}$, and choose the coordinate system so that the propagation direction is aligned with the z-axis, $\boldsymbol{k} = (0, 0, k)$, $n = k/k_0$. Maxwell's equations then give

$$\begin{pmatrix} \boldsymbol{D}_\perp \\ \boldsymbol{B}_\perp \end{pmatrix} - n\hat{P}\begin{pmatrix} \boldsymbol{E}_\perp \\ \boldsymbol{H}_\perp \end{pmatrix} = J_4,\ \hat{P} = \begin{pmatrix} 0 & 0 & 0 & -1 \\ 0 & 0 & 1 & 0 \\ 0 & 1 & 0 & 0 \\ -1 & 0 & 0 & 0 \end{pmatrix}$$

Let the rotated constitutive matrix be block-decomposed into the 4×4 block matrix $\widetilde{M}_\parallel$, 2×2 matrix $\widetilde{M}_z$, and rectangular matrices $\widetilde{M}_{\parallel z}$ and $\widetilde{M}_{z\parallel}$:

$$\widetilde{M} = \begin{pmatrix} \widetilde{M}_\parallel & \widetilde{M}_{\parallel z} \\ \widetilde{M}_{z\parallel} & \widetilde{M}_z \end{pmatrix}.$$

We introduce the 2D constitutive matrix $\hat{K}$ relating the transverse components of the fields:

$$\begin{pmatrix} \boldsymbol{D}_\perp \\ \boldsymbol{B}_\perp \end{pmatrix} = \hat{K}\begin{pmatrix} \boldsymbol{E}_\perp \\ \boldsymbol{H}_\perp \end{pmatrix},\ \text{such that } \left\{\hat{K} - n\hat{P}\right\}\begin{pmatrix} \boldsymbol{E}_\perp \\ \boldsymbol{H}_\perp \end{pmatrix} = J_4 \tag{9}$$

From Maxwell's equations we obtain the relationship between the 3D and 2D constitutive matrices $\hat{K} = \left\{\hat{M}_\parallel - \hat{M}_{\parallel z}\hat{M}_z^{-1}\hat{M}_{z\parallel}\right\}$ and the source vector:

$$\hat{J}_4 = \frac{4\pi i}{k_0 c}\left\{\begin{pmatrix} \boldsymbol{j}_{e\perp} \\ \boldsymbol{j}_{m\perp} \end{pmatrix} - \hat{M}_{\parallel z}\hat{M}_z^{-1}\begin{pmatrix} j_{ez} \\ j_{mz} \end{pmatrix}\right\}$$

We write

$$\hat{K} = \begin{pmatrix} \hat{\epsilon}^{(2)} & \hat{X}^{(2)} \\ \hat{Y}^{(2)} & \hat{\mu}^{(2)} \end{pmatrix},$$

and expand each 2×2 block in the natural 2D isotropic–antisymmetric–symmetric traceless basis of directional photonics parameters using the Pauli matrices $\hat{I}_2 = \sigma_0$, $\hat{S}_\perp = -i\sigma_y$, $\hat{\boldsymbol{A}}_\perp = (\sigma_z, \sigma_x)$.

Thus

$$\hat{\epsilon}^{(2)} = \epsilon_{\text{iso}}^{(2)}\hat{I}_2 + ig_e^{(2)}\hat{S}_\perp + \boldsymbol{a}_e^{(2)}\cdot\hat{\boldsymbol{A}}_\perp,\ \hat{\mu}^{(2)} = \mu_{\text{iso}}^{(2)}\hat{I}_2 + ig_\mu^{(2)}\hat{S}_\perp + \boldsymbol{a}_\mu^{(2)}\cdot\hat{\boldsymbol{A}}_\perp,$$

$$\hat{X}^{(2)} = \left(\chi^{(2)} - i\gamma^{(2)}\right)\hat{I}_2 + \left(V^{(2)} + i\Omega^{(2)}\right)\hat{S}_\perp + \left(\boldsymbol{a}_+^{(2)} - i\boldsymbol{a}_-^{(2)}\right)\cdot\hat{\boldsymbol{A}}_\perp,$$

$$\hat{Y}^{(2)} = \left(\chi^{(2)} + i\gamma^{(2)}\right)\hat{I}_2 + \left(-V^{(2)} + i\Omega^{(2)}\right)\hat{S}_\perp + \left(\boldsymbol{a}_+^{(2)} + i\boldsymbol{a}_-^{(2)}\right)\cdot\hat{\boldsymbol{A}}_\perp.$$

Here $\boldsymbol{a}^{(2)} = \left(a_1^{(2)}, a_2^{(2)}\right)$ are the coefficients of a symmetric traceless rank-two tensor in the transverse plane. The directional photonics parameters—the coefficients in this decomposition—are not global material parameters but effective parameters associated with the chosen direction $\hat{\boldsymbol{k}}$. Under a rotation of the transverse axes by the angle ϕ, the scalar and antisymmetric coefficients are invariant, while $\boldsymbol{a}^{(2)}$ transforms as

$$\begin{pmatrix} a_1' \\ a_2' \end{pmatrix} = \begin{pmatrix} \cos 2\phi & \sin 2\phi \\ -\sin 2\phi & \cos 2\phi \end{pmatrix}\begin{pmatrix} a_1 \\ a_2 \end{pmatrix}.$$

We rewrite Equation (9) in terms of the index-of-refraction operator $\hat{N} = \hat{P}^{-1}\left\{\hat{M}_{\parallel} - \hat{M}_{\parallel z}\hat{M}_z^{-1}\hat{M}_{z\parallel}\right\}$ as

$$\{\hat{N} - n\hat{I}\}\begin{pmatrix}\boldsymbol{E}_{\perp}\\ \boldsymbol{H}_{\perp}\end{pmatrix} = J_4$$

Following Refs. [18,29], we introduce the solution of this problem using the $\mathfrak{Z}_4$-potential:

$$\hat{J}_4 = F\mathfrak{Z}_4, \begin{pmatrix}\boldsymbol{E}_{\perp}\\ \boldsymbol{H}_{\perp}\end{pmatrix} = \hat{U}_4\mathfrak{Z}_4$$

where $F = \det\{\hat{N} - n\hat{I}\}$ and $\hat{U}_4 = \mathrm{adj}\{\hat{N} - n\hat{I}\}$.

In the absence of sources, $\hat{J}_4 = 0$ and the generalized eigenproblem $\{\hat{K} - n\hat{P}\}\begin{pmatrix}\boldsymbol{E}_{\perp}\\ \boldsymbol{H}_{\perp}\end{pmatrix} = 0$ converts into an ordinary eigenproblem for the index-of-refraction operator $\{\hat{N} - n\hat{I}\}\begin{pmatrix}\boldsymbol{E}_{\perp}\\ \boldsymbol{H}_{\perp}\end{pmatrix} = 0$. The operator $\hat{N}$ can be expressed using the 2D photonic parameters as

$$\hat{N} = \hat{N}_{\mathrm{iso}} \otimes \hat{I}_2 + \hat{N}^{(S)} \otimes \hat{S}_{\perp} + \hat{N}_x^{(A)} \otimes \sigma_x + \hat{N}_z^{(A)} \otimes \sigma_z,$$

where

$$\hat{N}_{\mathrm{iso}} = \begin{pmatrix} V^{(2)} - i\Omega^{(2)} & -ig_{\mu}^{(2)} \\ ig_{e}^{(2)} & V^{(2)} + i\Omega^{(2)} \end{pmatrix}, \hat{N}^{(S)} = \begin{pmatrix} \chi^{(2)} + i\gamma^{(2)} & \mu_{\mathrm{iso}}^{(2)} \\ -\epsilon_{\mathrm{iso}}^{(2)} & -\chi^{(2)} + i\gamma^{(2)} \end{pmatrix},$$

$$\hat{N}_x^{(A)} = \begin{pmatrix} a_{+,1}^{(2)} + ia_{-,1}^{(2)} & a_{\mu,1}^{(2)} \\ -a_{e,1}^{(2)} & -a_{+,1}^{(2)} + ia_{-,1}^{(2)} \end{pmatrix}, \hat{N}_z^{(A)} = \begin{pmatrix} -\left(a_{+,2}^{(2)} + ia_{-,2}^{(2)}\right) & -a_{\mu,2}^{(2)} \\ a_{e,2}^{(2)} & a_{+,2}^{(2)} - ia_{-,2}^{(2)} \end{pmatrix}.$$

Finally, Equation (8) for the bare Fresnel wave surfaces can be rewritten as [9]

$$F(n) = \det(\hat{N} - n\hat{I}) = 0, \text{that is, } n^4 - \mathrm{tr}(\hat{N})n^3 + \xi n^2 - \zeta n + \det(\hat{N}) = 0, \text{ with}$$

$$\xi = \frac{1}{2}\left[\left(\mathrm{tr}\hat{N}\right)^2 - \mathrm{tr}\left(\hat{N}^2\right)\right], \zeta = \frac{1}{6}\left[2\mathrm{tr}\left(\hat{N}^3\right) - 3\mathrm{tr}\left(\hat{N}^2\right)\mathrm{tr}\left(\hat{N}\right) + \left(\mathrm{tr}\hat{N}\right)^3\right].$$

The four roots of this quartic equation give the refractive-index branches for the chosen direction, and their collection over all directions defines the bare Fresnel wave surface.

3. OPV Exceptional Points and Separatrices

The boundaries between forward- and backward-wave propagation are the OPV separatrices, determined by the condition

$$\boldsymbol{k} \cdot \boldsymbol{S} \propto \boldsymbol{k} \cdot \frac{\partial F}{\partial \boldsymbol{k}} = 0,$$

which defines curves on the Fresnel wave surface $F(\boldsymbol{k}) = 0$ separating regions with opposite signs of $\boldsymbol{k} \cdot \boldsymbol{S}$. Mathematically, these curves correspond to the silhouette of the Fresnel wave surface. In differential geometry, silhouette curves are defined as the set of points where the viewing direction is tangent to the surface, or equivalently where the surface normal is orthogonal to the observation direction. In the present case, the surface normal is given by $\nabla_{\boldsymbol{k}} F$, and the condition $\boldsymbol{k} \cdot \nabla_{\boldsymbol{k}} F = 0$ identifies precisely those points where the wavevector

lies in the tangent plane to the Fresnel surface. Thus, these separatrices form the silhouette of the surface when viewed along $\boldsymbol{k}$.

Strikingly, these $\boldsymbol{k} \cdot \boldsymbol{S} = 0$ curves are not merely geometric features but correspond to genuine singularities of the index-of-refraction operator. They arise in completely Hermitian, lossless media, yet exhibit the defining algebraic signature of exceptional points: the coalescence of both index-of-refraction eigenvalues and polarization eigenvectors into a defective Jordan structure. This does not contradict the usual association of exceptional points with non-Hermitian systems, because the degeneracy here is not the degeneracy of a Hamiltonian. Rather, it is the degeneracy of the index-of-refraction operator $\hat{N}$, which generally need not be Hermitian even when the underlying electromagnetic medium is Hermitian.

These OPV exceptional points differ fundamentally from diabolical points. While both involve eigenvalue degeneracy, diabolical points preserve linearly independent eigenvectors and, therefore, remain diagonalizable. Ordinary diabolical degeneracies require the stronger condition $\frac{\partial F}{\partial \boldsymbol{k}} = 0$, corresponding to vanishing group velocity. In contrast, the OPV exceptional points identified here occur already under the weaker silhouette condition $\boldsymbol{k} \cdot \frac{\partial F}{\partial \boldsymbol{k}} = 0$, and are therefore directly tied to the transition between forward and backward propagation.

The condition $\boldsymbol{k} \cdot \frac{\partial F}{\partial \boldsymbol{k}} = \boldsymbol{k} \cdot \boldsymbol{S} = 0$ on the Fresnel wave surface corresponds, in the wave-rotated coordinate system, to the double-root condition $F(n) = \frac{dF}{dn} = 0$, and therefore to degenerate refractive-index branches. Indeed, for each direction of propagation, the resonance condition $F(n) = 0$ has four roots $n = n_1, \ldots, n_4$ corresponding to the four indices of refraction of the respective electromagnetic waves. The necessary and sufficient condition for a coalescence of two roots at $n_1 = n_2 = n_0$ is

$$F(n) = 0 \text{ and } \frac{dF}{dn} = 4n^3 - 3\mathrm{tr}\big(\hat{N}\big)n^2 + 2\xi \mathrm{n} - \zeta = 0$$

For a simple root $F(n) = (n - n_0)F'(n)$ with $F'(n_0) \neq 0$. However, for a double root $F(n) = (n - n_0)^2 F''(n)/2$ with $F''(n_0) \neq 0$, but $F'(n_0) = 0$.

Thus, the OPV condition is not only a geometric condition on the Fresnel wave surface, but also the algebraic condition for coalescence of refractive-index eigenvalues. When this root coalescence is accompanied by eigenvector coalescence of the generally non-Hermitian operator $\hat{N}$, the result is an OPV exceptional point in a Hermitian electromagnetic medium. The simplest example of when indices of refraction, as eigenvalues belonging to the spectrum of the operator $\hat{N}$, become complex in Hermitian media are lossless hyperbolic metamaterials.

As an initial illustration, let us consider the eigenvectors $(\boldsymbol{E}_\perp, \boldsymbol{H}_\perp)$ corresponding to the coalescent roots $n_1 = n_2 = n_0$. Assume first that both $\boldsymbol{E}_\perp$ and $\boldsymbol{H}_\perp$ are linearly polarized in the transverse xy-plane. On the OPV separatrix, $\boldsymbol{k} \cdot \boldsymbol{S} = 0$, so the longitudinal component of the Poynting vector vanishes. For linearly polarized transverse fields, this means that the directions of $\boldsymbol{E}_\perp$ and $\boldsymbol{H}_\perp$ coincide. By rotating the transverse coordinate system around $\hat{\boldsymbol{k}}$, this common transverse direction can be aligned with the x-axis. In that frame, the full $\boldsymbol{E}$ and $\boldsymbol{H}$ fields lie in the xz-plane, and the Abraham momentum axis is aligned with the y-axis, so that $\boldsymbol{S} \parallel \hat{\boldsymbol{y}}$. The eigenvector can then be written as $(\boldsymbol{E}_\perp, \boldsymbol{H}_\perp) = (Z_\perp, 0, 1, 0)$, where $Z_\perp = \frac{E_x}{H_x}$ is the transverse impedance. This impedance must be the same for both waves associated with the degenerate roots $n_1 = n_2 = n_0$. Indeed, it satisfies the linear equation $Z_\perp \hat{N}_1 + \hat{N}_3 = n_0 \left(Z_\perp, 0, 1, 0\right)^T$, where $\hat{N}_1$ and $\hat{N}_3$ are the first and third columns of $\hat{N}$. This equation admits at most one value of $Z_\perp$. Therefore, although the eigenvalue n_0 is doubly degenerate, the corresponding eigenspace is at most one-dimensional. The two roots $n_1 = n_2 = n_0$ thus share the same eigenvector, implying eigenvector coalescence and

defectiveness of $\hat{N}$ in an exceptional-point-like manner, but without requiring material loss or gain.

Consider a Hermitian reciprocal material with $\hat{\epsilon} = \mathrm{diag}\{-2, -1, 1\}$, $\hat{\mu} = \mathrm{diag}\{1, 2, -1\}$. This material has twelve diabolical singularities, as can be seen from the Fresnel wave surface of this material shown in Figure 2a. One of them, marked by a red dot, corresponds to the direction $\hat{\boldsymbol{k}} = \left(\sqrt{3/5}, 0, \sqrt{2/5}\right)$. The index-of-refraction operator for this direction is diagonalizable

$$\hat{N} = \begin{pmatrix} 0 & B \\ C & 0 \end{pmatrix}, \; B = \begin{pmatrix} 0 & 2 \\ 5 & 0 \end{pmatrix}, \; C = \begin{pmatrix} 0 & 1 \\ \frac{5}{2} & 0 \end{pmatrix}.$$

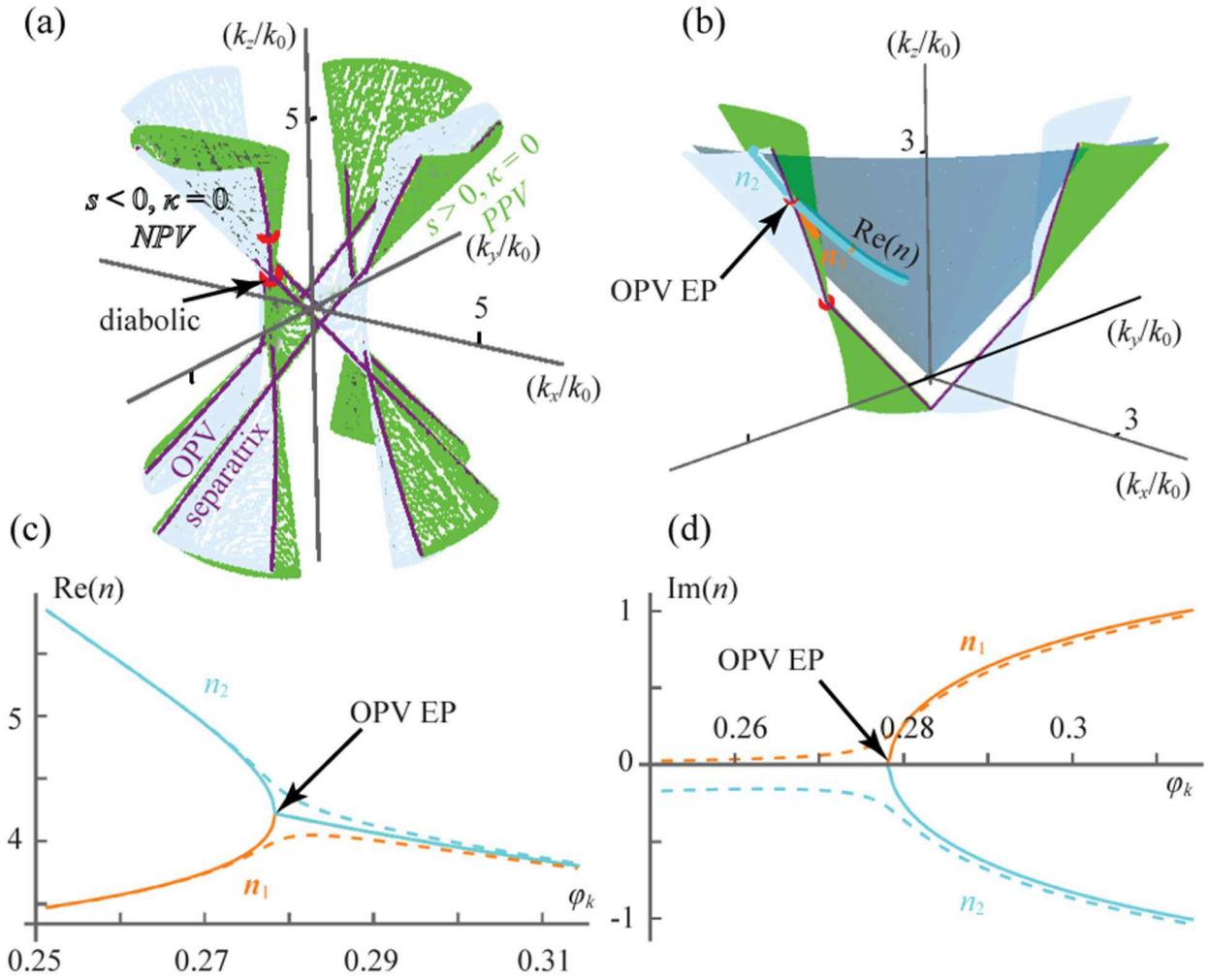


Figure 2. OPV separatrices and exceptional points. (**a**) Bare Fresnel wave surface for the Hermitian reciprocal material $\hat{\epsilon} = \mathrm{diag}(-2, -1, 1)$, $\hat{\mu} = \mathrm{diag}(1, 2, -1)$. The colored regions indicate PPV (green) and NPV (light blue) domains, while the purple curves show the OPV separatrices defined by $\boldsymbol{k} \cdot \boldsymbol{S} = 0$. Diabolical point and OPV EP discussed in the text are indicated by red dots. (**b**) Same as panel (**a**) but a close up of the OPV EP. The red point and black arrow mark the OPV EP, and the blue cone represents nearby propagation directions used to scan the refractive-index branches. The traces on the cone show $\mathrm{Re}(n_1)$ (cyan) and $\mathrm{Re}(n_2)$ (orange). (**c**) Real parts of the two refraction index branches as functions of the angular direction φ_k along the cone in (**b**). The indices of refraction coalesce at the OPV EP. The dashed lines show the unfolding of the OPV EP when a small loss perturbation is added: $\hat{M} \to \hat{M} + \delta\hat{M}$, $\delta\hat{M} = 10^{-3} i\, \hat{I}_6$. (**d**) Imaginary parts of the same branches, showing the exceptional-point-type unfolding of the refractive-index eigenvalues. The medium is Hermitian, but the degeneracy occurs in the generally non-Hermitian index-of-refraction operator $\hat{N}$.

Its eigenvalues are $n_i = \pm\sqrt{5}$ and it possesses four independent eigenvectors, $(\boldsymbol{E}_\perp, \boldsymbol{H}_\perp) = \left(\pm 2, 0, 0, \sqrt{5}\right)$, $\left(0, \pm\sqrt{5}, 1, 0\right)$. Thus, this is an ordinary diabolical degeneracy: the eigenvalues are degenerate, but the eigenspace remains complete.

By contrast, this is not true for the OPV exceptional points on the OPV separatrix. In Figure 2a, the green and light-blue regions show the two handedness domains on the bare Fresnel wave surface, with green denoting $s > 0$ PPV propagation and light blue denoting $s < 0$ NPV propagation. For the anisotropic material considered here, these PPV and NPV regions are associated with the electric-like and magnetic-like hyperbolic branches respectively identified in Ref. [30]. The purple curves show the OPV separatrices.

In Figure 2 we show the OPV separatrices using the purple curves. Consider, for example, the direction $\hat{\boldsymbol{k}} = \left(\frac{7}{\sqrt{107}}, \frac{2}{\sqrt{107}}, \frac{3\sqrt{6}}{\sqrt{107}}\right)$ and its intersection with the Fresnel wave surface also shown using a red dot. The corresponding index-of-refraction operator is

$$\hat{N} = \begin{pmatrix} 0 & B \\ C & 0 \end{pmatrix},\ B = \begin{pmatrix} -\sqrt{\frac{214}{3}} & -\frac{113}{3} \\ 0 & \sqrt{\frac{214}{3}} \end{pmatrix},\ C = \begin{pmatrix} -\frac{\sqrt{\frac{107}{6}}}{2} & -\frac{79}{24} \\ 0 & \frac{\sqrt{\frac{107}{6}}}{2} \end{pmatrix}.$$

This operator is defective. Its Jordan normal form is

$$\hat{N}_J = \begin{pmatrix} J_- & 0 \\ 0 & J_+ \end{pmatrix}, J_\pm = \begin{pmatrix} \pm n_0 & 1 \\ 0 & \pm n_0 \end{pmatrix}, n_0 = \frac{\sqrt{107}}{\sqrt{6}}.$$

The 4×4 operator $\hat{N}$ therefore has only two ordinary eigenvectors $\mathbf{v} = (\boldsymbol{E}_\perp, \boldsymbol{H}_\perp)$, with

$$\boldsymbol{H}_\perp = \left(-\frac{5\sqrt{2}}{321}, 1\right), \boldsymbol{E}_\perp = \pm 2\,\boldsymbol{H}_\perp, \text{ and } Z_\perp = \pm 2.$$

The corresponding generalized eigenvectors are

$$\mathbf{u} = (\boldsymbol{E}_\perp, \boldsymbol{H}_\perp) = \left(\frac{12}{107}, \frac{110}{7}\sqrt{\frac{2}{321}}, \pm\frac{424}{2247}, 0\right).$$

The red point in Figure 2b shows this OPV exceptional point on Fresnel wave surface. The blue cone defines a one-parameter family of nearby directions. Moving along this cone gives the angular coordinate φ_k used in Figure 2c,d. The real parts of the two refractive-index branches are traced directly on the cone in Figure 2b and then plotted as functions of φ_k in Figure 2c. At the OPV EP these two real branches coalesce, consistent with the double-root condition $F(n) = dF/dn = 0$. When a small non-Hermitian perturbation is added, the degeneracy unfolds: the real parts separate and the imaginary parts shown in Figure 2d become nonzero. This illustrates the sensitivity of the OPV EP to loss or gain perturbations. While the perturbation is small $\delta\hat{M} = 10^{-3} i\, \hat{I}_6$, the splitting is orders of magnitude larger, $|\delta n| \propto 0.1$.

In the Jordan-degenerate case, the index-of-refraction operator $\hat{N}$ admits an eigenvector $\mathbf{v}$ and a generalized eigenvector $\mathbf{u}$ satisfying

$$(\hat{N} - \lambda I)\mathbf{v} = 0,\ (\hat{N} - \lambda I)\mathbf{u} = \mathbf{v}.$$

The corresponding field solution takes the form of an OPV mode,

$$\psi(z) = e^{ik_0 \hat{N} z}\psi(0) = [(c_1 + ic_2 k_0 z)\mathbf{v} + c_2\mathbf{u}]e^{ik_0 n_0 z}.$$

This expression exhibits the characteristic linear-in-z prefactor associated with Jordan-block dynamics, formally analogous to the behavior at exceptional points. However, since $\boldsymbol{k} \cdot \boldsymbol{S} \neq 0$ for the generalized eigenvector $\mathbf{u}$, the condition $\boldsymbol{k} \cdot \boldsymbol{S} = 0$ is violated if $c_2 \neq 0$. In an unbounded Hermitian medium, where n_0 is real, the condition $c_2 = 0$ is therefore formally enforced; otherwise, the linear prefactor would produce unbounded amplitude growth, in contrast to Voigt-type solutions in non-Hermitian media [31].

Thus, although OPV singularities have the algebraic structure of exceptional points, they arise within Hermitian electromagnetic media and are intrinsically linked to the OPV separatrices, where forward- and backward-propagating domains meet. This gives the physical reason for OPV exceptional points. At OPV, $\boldsymbol{k} \cdot \boldsymbol{S} = 0$, so the transverse electric and magnetic fields no longer form the oriented-area structure that normally produces longitudinal Poynting flux. In the simplest case, they become parallel in the transverse plane. At the same time, OPV marks a turning point of the refractive-index branches for a fixed propagation direction. Thus, the loss of longitudinal energy flow is accompanied by a loss of polarization and impedance distinction between the coalescing modes, allowing the index-of-refraction operator $\hat{N}$ to become defective at the OPV exceptional point.

4. Gain–Loss Singularities and Separatrices

We now extend the propagation-map construction to non-Hermitian media. We introduce loss or gain by perturbing the Hermitian constitutive matrix $\hat{M}$ as

$$\hat{M}' = \hat{M} + \delta\hat{M},$$

where $\hat{M} = \hat{M}^\dagger$ describes the unperturbed lossless material and $\delta\hat{M}$ represents the non-Hermitian part of the response. In the photonic-parameter representation introduced above, this corresponds to allowing the material parameters to acquire complex corrections. The Maxwell operator is modified accordingly, $\hat{\mathcal{L}}' = \hat{Q} + i\omega\hat{M}'$, and the refractive index becomes complex,

$$n \to n + i\kappa.$$

The coefficient κ describes extinction or amplification and the most direct way to locate the boundary between these two behaviors is to impose $\kappa = 0$. At this boundary the refractive index is real, even though the medium is non-Hermitian. Therefore, the non-Hermitian dispersion equation $\det\hat{\mathcal{L}}' = 0$ must admit a real-k solution. Since $\det\hat{\mathcal{L}}'$ is generally complex, this gives the two real conditions

$$\mathrm{Re}\{\det\hat{\mathcal{L}}'\} = 0, \ \mathrm{Im}\{\det\hat{\mathcal{L}}'\} = 0. \tag{10}$$

This real/imaginary decomposition of a complex quartic dispersion condition was previously used in the inverse problem of quartic photonics, where complex bianisotropic media were represented through the intersection of analogous real and imaginary quartic surfaces [32]. In that work, the construction provided a way to relate prescribed complex photonic states to effective material parameters. Here, we use the same operational principle in a different context: the simultaneous solution of Equation (10) identifies real-k filaments on the non-Hermitian Fresnel wave surface. We interpret these filaments as gain–loss separatrices, because they mark the loci where the complex refractive index becomes real and the gain–loss character of the propagation map changes. The orange curve in Figure 1a corresponds to this type of separatrix.

The physical distinction between attenuation and amplification is not determined by the sign of κ alone, but by the sign of its product with the energy-flow component along the propagation direction, $\kappa S_z = \kappa s$. For a given propagation branch, $\kappa s > 0$ corresponds

to attenuation, while $\kappa s < 0$ corresponds to amplification. Thus, the gain–loss separatrix divides the non-Hermitian propagation map into dark and bright domains, corresponding respectively to decaying and amplified fields. The zeros of κ therefore define the boundaries at which the gain–loss character reverses.

These properties are illustrated in Figure 3, where the momentum-resolved DOS distribution ρ is shown for the $k_z = 0$ cross-section of the Fresnel wave surface from Figure 1a. The direction-dependent sign of the density of states, sign$\rho\left(\hat{\mathbf{k}}\right)$, is an important characteristic of the material. It indicates which waves transfer energy from external sources into the medium, corresponding to $\rho\left(\hat{\mathbf{k}}\right) > 0$ (absorption), and which correspond to the opposite direction of energy transfer, $\rho\left(\hat{\mathbf{k}}\right) < 0$ (gain) [18,33]. In Figure 3a the intersections of the curves $\mathrm{Re}\{\det\hat{\mathcal{L}}'\} = 0$, $\mathrm{Im}\{\det\hat{\mathcal{L}}'\} = 0$ are marked by black arrows and numbered 1–4. These intersections identify the real-k gain–loss separatrices and coincide with the sign changes in the DOS.

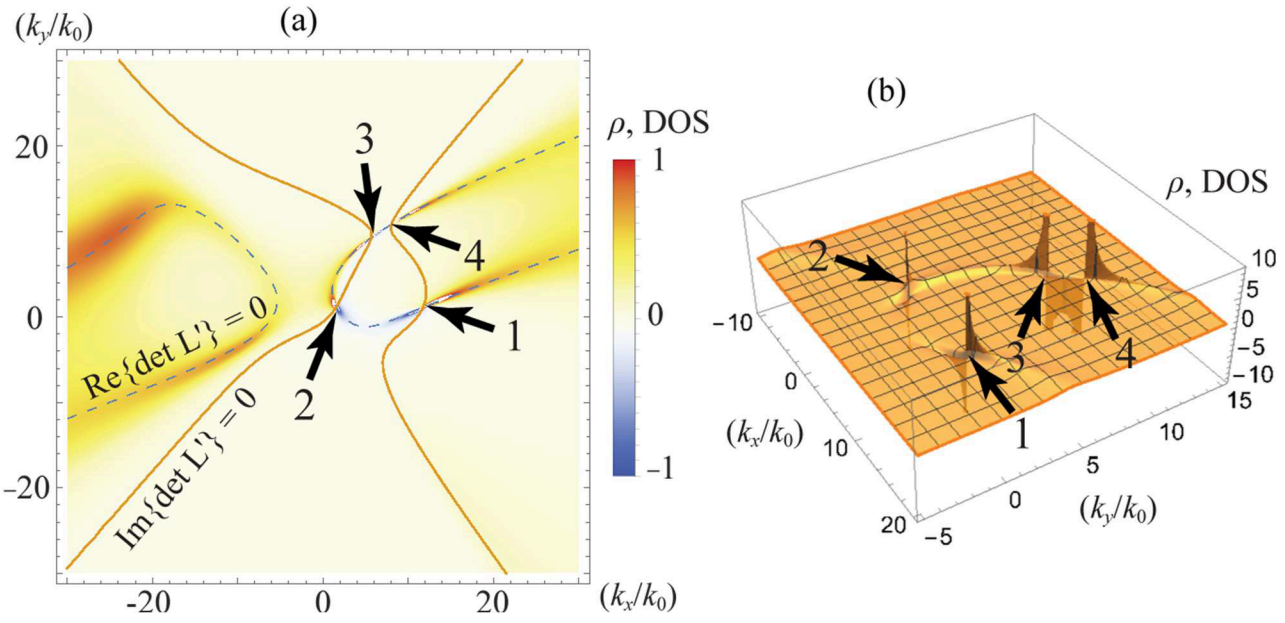


Figure 3. Gain–loss separatrices and momentum-resolved density of states in a non-Hermitian Fresnel wave-surface map. (**a**) Momentum-resolved density of states ρ in the $k_z = 0$ cross-section of the non-Hermitian Fresnel wave surface. The orange and dashed curves show the real and imaginary dispersion conditions, $\mathrm{Re}\{\det\hat{\mathcal{L}}'\} = 0$ and $\mathrm{Im}\{\det\hat{\mathcal{L}}'\} = 0$. Their intersections, marked by numbered arrows, define real-k filaments where $\kappa = 0$, corresponding to gain–loss separatrices. Across these curves the gain–loss character changes sign. (**b**) Three-dimensional view of the same DOS landscape. The peaks and sign changes illustrate how gain–loss singularities appear as gain–loss reversal points in the broadened momentum-resolved density of states.

The singular points associated with these $\kappa = 0$ curves are termed gain–loss singularities. At $\kappa = 0$, the phase-propagation direction remains continuous, while the gain–loss character, determined by the sign of κS_z, reverses across the gain–loss separatrix. In this sense, gain–loss singularities play for the non-Hermitian gain–loss map a role analogous to that played by OPV exceptional points for the Hermitian handedness switching.

The same condition can also be expressed perturbatively in terms of the fields. Expanding the determinant of the non-Hermitian Maxwell operator to first order gives

$$\det\hat{\mathcal{L}}' = \det(\hat{\mathcal{L}} + \delta\hat{\mathcal{L}}) = \det\hat{\mathcal{L}} + \mathrm{tr}\left[\mathrm{adj}(\hat{\mathcal{L}})\delta\hat{\mathcal{L}}\right].$$

On the unperturbed Fresnel surface, $\det\hat{\mathcal{L}} = 0$, so the non-Hermitian correction is governed by the projection of the perturbation onto the unperturbed mode. If $\mathbf{v} = (\boldsymbol{E}, \boldsymbol{H})$ is the eigenvector of the corresponding Hermitian mode, this correction may be written as $\mathrm{tr}\left[\mathrm{adj}\left(\hat{\mathcal{L}}\right)\delta\hat{\mathcal{L}}\right] \propto \mathbf{v}^T\delta\hat{M}\mathbf{v}$.

Equivalently, introducing the complex energy $U \propto \boldsymbol{E}\cdot\boldsymbol{D}^* + \boldsymbol{H}\cdot\boldsymbol{B}^*$ through $\mathrm{Im}(k)\,S_z = \mathrm{Im}(U), \mathrm{Re}(k)\,S_z = \mathrm{Re}(U)$, one obtains the quality factor of the electromagnetic wave as

$$Q^{-1} = \frac{\mathrm{Im}(k)}{\mathrm{Re}(k)} = \frac{\mathrm{Im}(U)}{\mathrm{Re}(U)}.$$

Using $k = k_0 n$, this gives

$$\kappa = n\,\frac{\mathrm{Im}(U)}{\mathrm{Re}(U)} = \frac{\mathrm{Im}(U)}{S_z}.$$

For a weak non-Hermitian perturbation $\delta\hat{M}$,

$$\delta n = i\kappa = n\,\frac{\mathbf{v}^T\delta\hat{M}\,\mathbf{v}}{\mathbf{v}^T\hat{M}\,\mathbf{v}}$$

Thus, the condition $\mathbf{v}^T\delta\hat{M}\mathbf{v} = 0$ is the perturbative field-based form of the more operational gain–loss separatrix condition Equation (10). In this sense, the determinant equations locate the separatrix directly, while the modal expression explains how a particular electromagnetic mode experiences the non-Hermitian perturbation. Together with the OPV separatrix $\boldsymbol{k}\cdot\boldsymbol{S} = 0$, the gain–loss separatrix completes the propagation map: one boundary separates PPV from NPV propagation, while the other separates attenuation from amplification.

5. Momentum-Resolved Density of States and OPV Gain–Loss Singularities

The addition of loss or gain gives the refractive-index branches imaginary parts

$$n_i \to n_i + i\kappa_i.$$

As a result, the delta-functional DOS of the bare Fresnel wave surface is broadened (see Figure 3 for illustration). In the Hermitian limit, the momentum-resolved density of states is concentrated on shell. In the non-Hermitian case, this delta function is replaced by a Lorentzian [18],

$$\rho\left(\hat{\boldsymbol{k}}\right) = \sigma\,\delta(k - k_0 n) \to \rho = \frac{\sigma}{\pi}\,\frac{k_0\kappa}{(k - k_0 n)^2 + (k_0\kappa)^2}.$$

Here $\sigma = \sigma\left(\hat{\boldsymbol{k}}\right), n = n\left(\hat{\boldsymbol{k}}\right), \kappa = \kappa\left(\hat{\boldsymbol{k}}\right)$ are direction-dependent quantities: σ is the surface-density-of-states prefactor, n is the real part of the refractive index, and κ is the extinction/amplification coefficient. From the Lorentzian form above the sign of the broadened DOS can be expressed as

$$\mathrm{sign}\,\rho = \mathrm{sign}\,\sigma\mathrm{sign}\,\kappa. \tag{11}$$

Following Appendix B, the surface-density prefactor σ can be written as

$$\sigma = \frac{6\omega^3}{c^3}n_0^3\left(\frac{E_x^2}{\boldsymbol{E}\cdot\boldsymbol{D}^* + \boldsymbol{H}\cdot\boldsymbol{B}^*}\right) = \frac{6\omega^2}{c^2}n_0^3\left(\frac{E_x^2}{2\boldsymbol{k}\cdot\mathrm{Re}\{\boldsymbol{E}\times\boldsymbol{H}^*\}}\right)$$

The sign of SDOS, sign $\sigma = \text{sign}(\boldsymbol{k} \cdot \boldsymbol{S})$, means that for right-handed waves $\sigma > 0$, while for left-handed waves $\sigma < 0$. The relation in Equation (11) helps combine the two sign structures of the propagation map: the factor σ carries the handedness information through $\boldsymbol{k} \cdot \boldsymbol{S}$, while κ carries the information about the gain–loss due to the non-Hermitian perturbation

It is noteworthy that, similarly to σ, the sign of the extinction coefficient κ is governed by the sign of $\boldsymbol{k} \cdot \boldsymbol{S} \propto \mathbf{v}^T \hat{M} \mathbf{v}$. As a result, κ changes sign upon crossing an OPV exceptional point, so that modes on opposite sides of a OPV separatrix possess opposite extinction. Consequently, according to Equation (11) the sign of the density of states ρ and loss–gain state remains unchanged across OPV separatrices and only changes at gain–loss singularities:

$$\text{sign}\, \rho = \text{sign}\, \kappa s. \tag{12}$$

The defining feature of OPV exceptional points is $\boldsymbol{k} \cdot \boldsymbol{S} = 0$, which leads to divergence of the surface density of states (SDOS), $\sigma \propto (\boldsymbol{k} \cdot \boldsymbol{S})^{-1} \to \infty$. Nevertheless, the significance of this is reduced by the fact that for Hermitian media this divergence adds to the already divergent delta-functional momentum-resolved DOS distribution. In non-Hermitian media, this divergence is generally unfolded by perturbations of the OPV EP, as illustrated in Figure 2.

Gain–loss singularities produce a more dramatic DOS signature. Since gain–loss singularities occur at $\kappa = 0$, they correspond to points where the Lorentzian linewidth $k_0\kappa$ of the momentum-resolved spectral response collapses. At the on-shell momentum $k = k_0 n$, the Lorentzian amplitude scales as

$$\rho(k = k_0 n) \sim \frac{\sigma}{\pi k_0 \kappa},$$

so the DOS develops a sharp peak whose sign reverses across the gain–loss singularity, as illustrated in Figure 3b, where four gain–loss singularities are marked by black arrows. Thus, a gain–loss singularity is not only a boundary between attenuation and amplification; it is a threshold-like momentum-space singularity of the non-Hermitian Fresnel wave-surface map. Its origin stems from the vanishing of the non-Hermitian linewidth of the dressed Fresnel wave surface. In this sense, gain–loss singularities identify directions in momentum space where the exchange of energy between the field and the medium reverses sign. All numerical figures in this work were generated using custom-written numerical routines. No commercial full-wave solver was used. For each chosen constitutive matrix $\hat{M}$, the direction-dependent reduced index-of-refraction operator $\hat{N}$ was constructed, and the quartic equation $\det(\hat{N} - n\hat{I}) = 0$ was solved as a function of propagation direction. The corresponding eigenvectors were then used to evaluate the Poynting vector, the signs of $\boldsymbol{k} \cdot \boldsymbol{S}$ and κs, the OPV separatrices, and the gain–loss/DOS-related quantities plotted in the figures.

6. Conclusions

We have shown that Fresnel wave surfaces can be interpreted as propagation maps that organize both handedness and gain–loss behavior. In Hermitian media, the OPV separatrices $\boldsymbol{k} \cdot \boldsymbol{S} = 0$ separates PPV and NPV domains and supports OPV exceptional points, where the index-of-refraction operator becomes defective even though the material medium remains Hermitian. In non-Hermitian media, the gain–loss separatrix is defined by real-k solutions of the complex dispersion equation,

$$\text{Re}\{\det\hat{\mathcal{L}}'\} = 0,\ \text{Im}\{\det\hat{\mathcal{L}}'\} = 0,$$

and marks the reversal between attenuation and amplification. The associated gain–loss singularities occur where the handedness remains continuous while the gain–loss character changes sign. Their physical importance is amplified by the momentum-resolved density of states: at $\kappa = 0$, the Lorentzian linewidth of the non-Hermitian momentum-resolved response collapses, producing a sharp peak in momentum-resolved DOS whose sign reverses across the separatrix, as illustrated in Figure 3b. Thus, gain–loss singularities are threshold-like gain–loss singularities of the Fresnel wave-surface propagation map, generated by non-Hermitian linewidth collapse. Together, OPV and gain–loss structures provide compact geometric language for describing how handedness, degeneracy, loss, gain, and momentum-resolved DOS are organized on Fresnel wave surfaces.

Funding: This research received no external funding.

Data Availability Statement: All data is included in the manuscript and is available upon reasonable request.

Conflicts of Interest: The authors declare no conflict of interest.

Appendix A. Photonic Material Parameters Retrieval

Using Equations (2)–(5) we obtain the isotropic parts as

$$\epsilon_{iso} = \frac{\mathrm{tr}(\hat{\epsilon})}{3},\ \mu_{iso} = \frac{\mathrm{tr}(\hat{\mu})}{3},\ \chi = \frac{1}{3}\,\mathrm{tr}\left(\frac{\hat{X}+\hat{Y}}{2}\right),\ \gamma = \frac{1}{3}\,\mathrm{tr}\left(\frac{i(\hat{X}-\hat{Y})}{2}\right).$$

Thus, ϵ_{iso} and μ_{iso} describe the isotropic electric and magnetic response, while χ and γ are the isotropic Tellegen and chiral magnetoelectric couplings, respectively.

The antisymmetric parts of $\hat{\epsilon}$ and $\hat{\mu}$, projected onto the spin-1 basis $\boldsymbol{S}$, define the gyroelectric and gyromagnetic vectors $\boldsymbol{g}_\epsilon$ and $\boldsymbol{g}_\mu$:

$$(g_\epsilon)_i = -\frac{1}{2}\,\mathrm{tr}[(-iS_i)\,\hat{\epsilon}],\ (g_\mu)_i = -\frac{1}{2}\,\mathrm{tr}[(-iS_i)\hat{\mu}],\ i = 1,2,3.$$

These three-component vectors encode the antisymmetric electric and magnetic response sectors.

For the magnetoelectric tensor combinations the antisymmetric spin-1 projections define the vectors $\boldsymbol{V}$ and $\boldsymbol{\Omega}$:

$$V_i = -\frac{1}{2}\,\mathrm{tr}\left[(-iS_i)\left(\frac{\hat{X}+\hat{Y}}{2}\right)\right],\ \Omega_i = -\frac{1}{2}\,\mathrm{tr}\left[(-iS_i)\left(\frac{i(\hat{X}-\hat{Y})}{2}\right)\right],\ i = 1,2,3.$$

In this parametrization, $\boldsymbol{V}$ describes the nonreciprocal moving-medium-type coupling, whereas $\boldsymbol{\Omega}$ corresponds to the reciprocal omega-type magnetoelectric coupling.

The remaining anisotropic contributions are contained in the symmetric traceless coefficients $\boldsymbol{a}_\epsilon, \boldsymbol{a}_\mu, \boldsymbol{a}_+, \boldsymbol{a}_-$, obtained by projection onto the five-element basis $\mathbf{A}$:

$$(a_e)_j = \frac{1}{2}\,\mathrm{tr}\big(A_j\hat{\epsilon}\big),\ (a_\mu)_j = \frac{1}{2}\,\mathrm{tr}\big(A_j\hat{\mu}\big),\ (a_+)_j = \frac{1}{2}\,\mathrm{tr}\left(A_j\left(\frac{\hat{X}+\hat{Y}}{2}\right)\right),\ (a_-)_j = \frac{1}{2}\,\mathrm{tr}\left(A_j\left(\frac{i(\hat{X}-\hat{Y})}{2}\right)\right),\ j = 1,\ldots,5.$$

These coefficients describe the symmetric traceless anisotropic parts of the electric, magnetic, and magnetoelectric response tensors.

In this way, the full constitutive response is decomposed into three parts: an isotropic part proportional to $\hat{I}_3$, an antisymmetric spin-1 part expanded in $\boldsymbol{S}$, and a symmetric traceless part expanded in $\boldsymbol{A}$.

Appendix B. Surface Density of States (SDOS)

Consider the operator $\hat{\Sigma}(\lambda) = \frac{\hat{L}}{ik} = \left(\frac{\hat{Q}}{k} + \lambda\hat{M}\right)$, where $\lambda = 1/n$. Near the Fresnel wave surface $\lambda \approx \lambda_0$ we expand

$$\hat{\Sigma}(\lambda) = \hat{\Sigma}(\lambda_0) + (\lambda - \lambda_0)\hat{M} + \cdots$$

$$\hat{\Sigma}^{-1}(\lambda) = \frac{\hat{\Sigma}_{-1}}{\lambda - \lambda_0} + \hat{\Sigma}_0 + \cdots$$

$$\hat{1} = \hat{\Sigma}(\lambda)\,\hat{\Sigma}^{-1}(\lambda) = \{\hat{\Sigma}(\lambda_0) + (\lambda - \lambda_0)\hat{M} + \cdots\}\left\{\frac{\hat{\Sigma}_{-1}}{\lambda - \lambda_0} + \hat{\Sigma}_0 + \cdots\right\}$$

From this $\hat{\Sigma}(\lambda_0)\hat{\Sigma}_{-1} = 0$, since the left-hand side has no pole at Fresnel wave surface. This means that each column of $\hat{\Sigma}_{-1}$ is a multiple of the nullvector $\mathbf{v}$ of $\hat{\Sigma}(\lambda_0)$: $\hat{\Sigma}_{-1} = \mathbf{v} \otimes \boldsymbol{\alpha}^T$, where $\boldsymbol{\alpha}$ is some unknown vector. This results in

$$\hat{\Sigma}(\lambda_0)\hat{\Sigma}_0 + \hat{M}\hat{\Sigma}_{-1} = \hat{1}$$

Multiplying by the left null vector $\mathbf{w}^T$ and using $\mathbf{w}^T\hat{\Sigma}(\lambda_0) = 0$, we get $\mathbf{w}^T\hat{M}(\mathbf{v} \otimes \boldsymbol{\alpha}^T) = \boldsymbol{w}^T$ or

$$\left(\mathbf{w}^T\hat{M}\,\mathbf{v}\right)\boldsymbol{\alpha}^T = \mathbf{w}^T,\ \boldsymbol{\alpha}^T = \frac{\mathbf{w}^T}{\mathbf{w}^T\hat{M}\,\mathbf{v}}.$$

Finally,

$$\hat{\Sigma}^{-1}(\lambda) = \frac{\mathbf{v} \otimes \mathbf{w}^T}{(\lambda - \lambda_0)\,\left(\mathbf{w}^T\hat{M}\,\mathbf{v}\right)}$$

For Hermitian materials $w = v = (\boldsymbol{E}, \boldsymbol{H})$, therefore

$$L^{-1} = -\frac{ikn_0^2}{(n - n_0)}\left(\frac{\mathbf{v} \otimes \mathbf{v}^T}{\mathbf{v}^T\hat{M}\,\mathbf{v}}\right) = -ik_0\frac{n_0^3}{(n - n_0)}\left(\frac{\mathbf{v} \otimes \mathbf{v}^T}{\mathbf{v}^T\hat{M}\,\mathbf{v}}\right)$$

From this

$$\rho = \frac{6\omega}{\pi c^2}\mathrm{Im}\{\hat{G}_{xx}\} = \frac{6\omega^2}{\pi c^2}\,\mathrm{Re}\left\{\left(\hat{L}^{-1}\right)_{xx}\right\} = \frac{6\omega^3}{\pi c^3}n_0^3\left(\frac{E_x^2}{\boldsymbol{E}\cdot\boldsymbol{D}^* + \boldsymbol{H}\cdot\boldsymbol{B}^*}\right)\mathrm{Im}\left\{\frac{1}{n - n_0}\right\}$$

The resulting expression for the prefactor σ is

$$\sigma = \frac{6\omega^3}{c^3}n_0^3\left(\frac{E_x^2}{\boldsymbol{E}\cdot\boldsymbol{D}^* + \boldsymbol{H}\cdot\boldsymbol{B}^*}\right) = \frac{6\omega^2}{c^2}n_0^3\left(\frac{E_x^2}{2\boldsymbol{k}\cdot\mathrm{Re}\{\boldsymbol{E}\times\boldsymbol{H}^*\}}\right)$$

References

1. Kong, J.A. *Electromagnetic Wave Theory*; EMW Publishing: Cambridge, MA, USA, 2008.
2. Hehl, F.W.; Obukhov, Y.N. *Foundations of Classical Electrodynamics: Charge, Flux, and Metric*; Birkhäuser: Boston, MA, USA, 2003.
3. Lakhtakia, A. *Beltrami Fields in Chiral Media*; World Scientific: Singapore, 1994.
4. Lindell, I.V.; Sihvola, A.H.; Tretyakov, S.A.; Viitanen, A.J. *Electromagnetic Waves in Chiral and Bi-Isotropic Media*; Artech House: Boston, MA, USA, 1994.
5. Serdyukov, A.; Semchenko, I.; Tretyakov, S.; Sihvola, A. *Electromagnetics of Bi-Anisotropic Materials: Theory and Applications*; Gordon and Breach: Amsterdam, The Netherlands, 2001.
6. Mackay, T.G.; Lakhtakia, A. *Electromagnetic Anisotropy and Bianisotropy: A Field Guide*, 2nd ed.; World Scientific: Singapore, 2019.
7. Eroglu, A. *Wave Propagation and Radiation in Gyrotropic and Anisotropic Media*; Springer: New York, NY, USA, 2010.
8. Poddubny, A.; Iorsh, I.; Belov, P.; Kivshar, Y. Hyperbolic metamaterials. *Nat. Photonics* **2013**, *7*, 948–957. [CrossRef]
9. Durach, M.; Williamson, R.; Laballe, M.; Mulkey, T. Tri- and tetrahyperbolic isofrequency topologies complete classifications of bianisotropic materials. *Appl. Sci.* **2020**, *10*, 763. [CrossRef]

10. Tuz, V.R.; Fesenko, V.I.; Fedorin, I.V.; Sun, H.-B.; Shulga, V.M.; Han, W. Dispersion peculiarities of hybrid modes in a circular waveguide filled by a composite gyroelectromagnetic medium. *J. Electromagn. Waves Appl.* **2017**, *31*, 140–154. [CrossRef]
11. Ra'di, Y.; Grbic, A. Magnet-free nonreciprocal bianisotropic metasurfaces. *Phys. Rev. B* **2016**, *94*, 195432. [CrossRef]
12. Deck-Léger, Z.-L.; Zheng, X.; Caloz, C. Electromagnetic wave scattering from a moving medium with stationary interfaces. *Photonics* **2021**, *8*, 202. [CrossRef]
13. Jazi, S.S.; Faniayeu, I.; Cichelero, R.; Tzarouchis, D.C.; Asgari, M.M.; Dmitriev, A.; Fan, S.; Asadchy, V. Optical Tellegen metamaterial with spontaneous magnetization. *Nat. Commun.* **2024**, *15*, 1854. [CrossRef]
14. Yang, Q.; Wen, X.; Li, Z.; You, O.; Zhang, S. Gigantic Tellegen responses in metamaterials. *Nat. Commun.* **2025**, *16*, 151. [CrossRef] [PubMed]
15. Feng, L.; El-Ganainy, R.; Ge, L. Non-Hermitian photonics based on parity–time symmetry. *Nat. Photonics* **2017**, *11*, 752–762. [CrossRef]
16. El-Ganainy, R.; Khajavikhan, M.; Ge, L. The dawn of non-Hermitian optics. *Commun. Phys.* **2019**, *2*, 37. [CrossRef]
17. Fesenko, V.I.; Tuz, V.R. Lossless and loss-induced topological transitions of isofrequency surfaces in a biaxial gyroelectromagnetic medium. *Phys. Rev. B* **2019**, *99*, 094404. [CrossRef]
18. Durach, M.; Keene, D. Beyond Fresnel wave surfaces: Theory of off-shell photonic density of states and near-fields in isotropy-broken materials with loss or gain. *Photonics* **2025**, *12*, 1032. [CrossRef]
19. Knörrer, H. The Fresnel wave surface. In *Geometry of Surfaces*; Lecture Notes in Mathematics; Springer: Berlin, Germany, 1984; Volume 1062, pp. 127–132.
20. Guo, Q.; Gao, W.; Chen, J.; Liu, Y.; Zhang, S. Line degeneracy and strong spin-orbit coupling of light with bulk bianisotropic metamaterials. *Phys. Rev. Lett.* **2015**, *115*, 067402. [CrossRef] [PubMed]
21. Favaro, A.; Hehl, F.W. Light propagation in local and linear media: Fresnel-Kummer wave surfaces with 16 singular points. *Phys. Rev. A* **2016**, *93*, 013844. [CrossRef]
22. Berry, M.V. The optical singularities of bianisotropic crystals. *Proc. R. Soc. A Math. Phys. Eng. Sci.* **2005**, *461*, 2071–2098. [CrossRef]
23. Miri, M.-A.; Alù, A. Exceptional points in optics and photonics. *Science* **2019**, *363*, eaar7709. [CrossRef]
24. Özdemir, Ş.K.; Rotter, S.; Nori, F.; Yang, L. Parity–time symmetry and exceptional points in photonics. *Nat. Mater.* **2019**, *18*, 783–798. [CrossRef]
25. Bergholtz, E.J.; Budich, J.C.; Kunst, F.K. Exceptional topology of non-Hermitian systems. *Rev. Mod. Phys.* **2021**, *93*, 015005. [CrossRef]
26. Mackay, T.G.; Lakhtakia, A.; Setiawan, S. Positive-, negative-, and orthogonal-phase-velocity propagation of electromagnetic plane waves in a simply moving medium. *Optik* **2007**, *118*, 195–202. [CrossRef]
27. Landau, L.D.; Lifshitz, E.M. *Electrodynamics of Continuous Media*, 2nd ed.; Pergamon Press: Oxford, UK, 1984.
28. Wilson, R. *Four Colors Suffice: How the Map Problem Was Solved*; Princeton University Press: Princeton, NJ, USA, 2002.
29. Durach, M. Beyond Green's Functions: Inverse Helmholtz and 'Om' ॐ-Potential Methods for Macroscopic Electromagnetism in Isotropy-Broken Media. *Photonics* **2025**, *12*, 660. [CrossRef]
30. Durach, M. Tetra-hyperbolic and tri-hyperbolic optical phases in anisotropic metamaterials without magnetoelectric coupling due to hybridization of plasmonic and magnetic Bloch high-*k* polaritons. *Opt. Commun.* **2020**, *476*, 126349. [CrossRef]
31. Mackay, T.G.; Lakhtakia, A. On the anatomy of Voigt plane waves. In *Adventures in Contemporary Electromagnetic Theory*; Springer: Cham, Switzerland, 2023; pp. 61–91.
32. Mulkey, T.; Dillies, J.; Durach, M. Inverse problem of quartic photonics. *Opt. Lett.* **2018**, *43*, 1226–1229. [CrossRef] [PubMed]
33. Park, J.; Lee, K.; Zhang, R.-Y.; Park, H.-C.; Ryu, J.-W.; Cho, G.Y.; Lee, M.Y.; Zhang, Z.; Park, N.; Jeon, W.; et al. Spontaneous emission decay and excitation in photonic time crystals. *Phys. Rev. Lett.* **2025**, *135*, 133801. [CrossRef] [PubMed]

Disclaimer/Publisher's Note: The statements, opinions and data contained in all publications are solely those of the individual author(s) and contributor(s) and not of MDPI and/or the editor(s). MDPI and/or the editor(s) disclaim responsibility for any injury to people or property resulting from any ideas, methods, instructions or products referred to in the content.